Hydrology and
Earth System
Sciences

Simulating the connections of ENSO and the rainfall regime of East Africa and the upper Blue Nile region using a climate model of the Tropics

M. A. H. Zaroug[1,2,5], F. Giorgi[1], E. Coppola[1], G. M. Abdo[3], and E. A. B. Eltahir[4]

[1]International Centre for Theoretical Physics, Earth System Physics, Trieste, Italy
[2]Dinder Centre for Environmental Research, Khartoum, Sudan
[3]University of Khartoum, Faculty of Engineering, Water Research Centre, Khartoum, Sudan
[4]Massachusetts Institute of Technology, Civil and Environmental Engineering, Cambridge, MA, USA
[5]The Hydraulics Research Center, Medani, Sudan

Correspondence to: M. A. H. Zaroug (modathir_23@yahoo.com)

Abstract. We simulate the observed statistical relationship between ENSO and the rainfall regime of the upper Blue Nile using the tropical-band version of the regional climate model RegCM4 (or Reg-TB). An ensemble of nine simulations for the 28-year period 1982–2009 is completed to investigate the role of ENSO in modulating rainfall over the upper Blue Nile catchment. Reg-TB shows a good skill in simulating the climatology of temperature, outgoing long-wave radiation patterns as well as related atmospheric circulation features during the summer season (i.e. the rainy season over the Blue Nile catchment). The model also succeeds in reproducing the observed negative correlation between Pacific SST and rainfall anomalies over the Blue Nile catchment, and in particular the association of droughts over the Blue Nile with El Niño events that start in April–June. We thus propose that observations and model forecasts of Pacific SST during this season could be used in seasonal forecasting of summer rainfall over the upper Blue Nile region.

1 Introduction

The Blue Nile has a great impact on the life of millions of people in Ethiopia, Sudan and Egypt. It originates from Lake Tana and descends from the Ethiopian high plateau, with many tributaries in its upper course across the Ethiopian Highlands and two more tributaries (Dinder and the Rahad) in its lower course across Sudan. Although the Blue Nile is relatively short compared to the White Nile and it has a relatively small drainage area, it carries 60 to 70 % of the total discharge and a great amount of sediment (Dumont, 2009).

During the last few decades, there has been a wide recognition that natural oscillations in the state of the Pacific Ocean have a significant impact on the patterns of weather and climate around the world (Diaz et al., 2001; Holton et al., 1989; Ropelewski and Halpert, 1987). Dominant among these oscillations is the El Niño–Southern Oscillation (ENSO) which has a period of about 4 years. ENSO is the largest contributor to inter-annual climate variability in the tropical Pacific as well as in remote regions around the globe (e.g. Müller and Roeckner, 2008). Eltahir (1996) found that 25 % of the natural variability in the annual flow of the Nile is associated with ENSO and proposed use of this observed correlation to improve the predictability of the Nile floods. Wang and Eltahir (1999) recommended an empirical methodology for medium and long-range (∼ 6 months) forecasting of the Nile floods using ENSO information, while Amarasekera et al. (1997) showed that ENSO episodes were negatively correlated with the floods of the Blue Nile and Atbara rivers during the period of 1912 to 1972. In addition, Eltahir (1996) showed that the probability of having a low (high) flood given cold ENSO Sea Surface Temperature (SST) conditions is 2 % (49 %), while the probability of having a high (low) flood given a warm ENSO SST condition is 8 % (58 %).

Some recent studies divided Ethiopia into regions according to the variability of rainfall seasonality and used observational data sets to study the impact of SST on the rainfall in the Ethiopian Highlands (Segele and Lamb, 2005; Seleshi and Zanke, 2004; Gissila et al., 2004). Other studies concentrated on East Africa but in regions outside the Ethiopian Highland, and showed negative correlation with ENSO in central and southern Sudan (Osman et al., 2001; Elagib and Elhag, 2001; Osman and Shamseldin, 2002).

These previous studies were conducted using observational data sets of SST, rainfall and river flow. In this study, we assess whether these observed connections between precipitation in the East Africa/Blue Nile region and SSTs in the Pacific Ocean can be reproduced by using a physically based model of the climate system (the Regional Climate Model RegCM4 in its tropical band configuration, Reg-TB, Giorgi et al., 2012; Coppola et al., 2012). Towards this purpose we completed and analysed an ensemble of nine simulations of tropical climate driven by observed SSTs and north–south boundary conditions from the ERA-Interim reanalysis of observations for the 28-year period 1982–2009. In particular, the analysis addresses the impact of ENSO on the precipitation regime in Eastern Africa and the catchment of the Blue Nile, with a focus on the summer rainy season over the region.

In Sect. 2 we describe model and experiment design, while in Sect. 3 we validate the model climatology over the Africa region of interest in this study. In Sect. 4 we then assess the representation of the connections between ENSO and precipitation in the Blue Nile River Basin. Final considerations are then provided in Sect. 5.

2 RegCM4 description, experiments and data

One of the new developments of RegCM4 (Giorgi et al., 2012) is the tropical band configuration described by Coppola et al. (2012), or Reg-TB, by which the model domain covers the entire tropical belt with periodic boundary conditions in the x-direction and relaxation boundary conditions at the southern and northern boundaries. Figure 1 shows the model domain and topography along with some sub-regions selected for more detailed regional analysis. For our experiments the horizontal resolution is approximately 125 km at the equator, i.e. 360 grid points. In the north–south direction the domain extends to about ± 45 degrees and 18 sigma layers are used in the vertical, as in the model standard configuration. The red rectangle in the Pacific Ocean represents the Niño 3.4 region, whereas the small square over Ethiopia represents our main focus area, i.e. the catchment of the upper Blue Nile.

For our experiments we used the following physics options described in Giorgi et al. (2012): modified CCM3 radiative transfer scheme (Kiehl et al., 1996), modified planetary boundary layer scheme (Holtslag et al., 1990), SUBEX

resolvable precipitation scheme (Pal et al., 2000), mixed cumulus convection configuration utilizing the scheme of Grell (1993) over land and that of Emanuel (1991) over oceans, and the biosphere–atmosphere transfer scheme (Dickinson et al., 1993) land surface package. As mentioned, the model uses forcing lateral boundary conditions only in the northern and southern boundaries of the domain, with no external forcing in an east–west direction. The initial and lateral boundary conditions are provided by the ERA-Interim $1.5° \times 1.5°$ gridded reanalysis (ERAI, Dee et al., 2011), which is the third-generation ECMWF reanalysis product. SSTs are from the weekly, $1°$ resolution Optimum Interpolation (OI) SST data set from the National Oceanic and Atmospheric Administration (Reynolds et al., 2007). The simulation period is from 1 January 1982 to 31 March 2010 (28 years) and nine ensemble members are completed. The difference between the nine members is in the initial day of the simulation, which varies by 1 day. The first member starts on 1 January 1982, the second on 2 January 1982 and so on until the ninth member starts on 9 January 1982. The observed data mainly used for model validation are from the Global Precipitation Climatology Project (GPCP) version 2.2 (Huffman et al., 2011), available from January 1979 to December 2010 with a resolution of 2.5°, although land data from the Climate Research Unit (CRU, land only, $0.5° \times 0.5°$ resolution; Mitchell et al., 2004) is also used for more detailed regional analysis.

Finally, we point out that in our analysis we mostly focus on ensemble averaged results in order to filter out the internal variability of the model from the forced signal associated with the SST forcing (Shukla et al., 2000). We however also show some examples of the spread across the ensemble members to provide a first-order assessment of this variability.

3 Validation of the model climatology over East Africa

In this section we first present a basic validation of the model climatology during the June–July–August–September (JJAS) rainy season over the broad East Africa region by comparing averages taken over the entire nine-member ensemble with available observations. Note that this model configuration is the same as that used by Coppola et al. (2012), and in that paper an assessment is provided of the model climatology over the entire tropical belt. In this regard, Coppola et al. (2012) show that, although regional biases in the model are present, the basic model climatology of equatorial and tropical regions is realistic. We also recall that, although we only analyse here data from the African region, the model is run for the full tropical band with forcing only at the northern and southern boundary, and therefore it is quite free to develop its own regional circulations and teleconnections within this large domain.
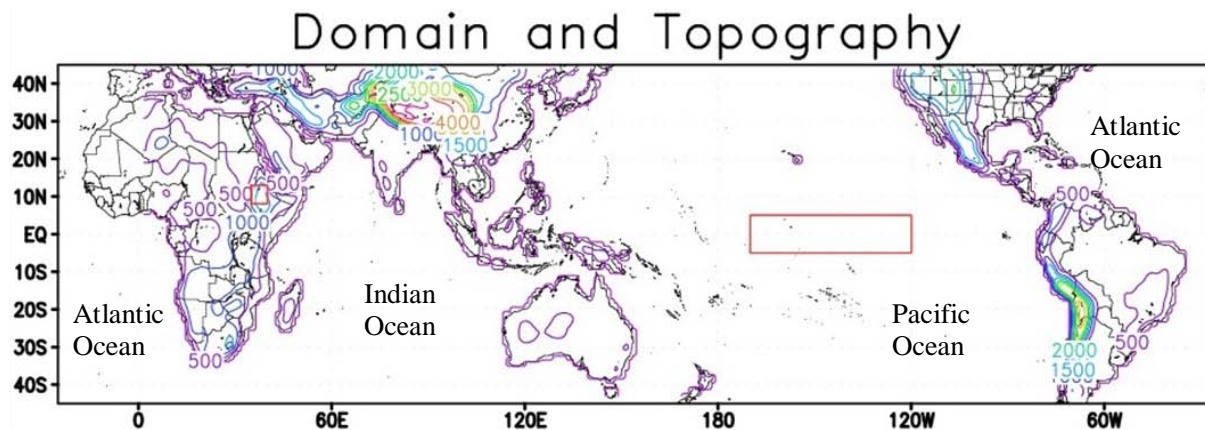
Figure 1. The domain and the topography of the model. The red box in the Pacific Ocean shows the Niño 3.4 region, while the red box in the Ethiopian Highlands shows the upper catchment of the Blue Nile (as in all following figures).

3.1 Rainfall

The spatial pattern of JJAS rainfall is compared to observations (both CRU and GPCP) in Fig. 2. In JJAS the ITCZ is located in the Northern Hemisphere, therefore rainfall over the continent is mostly confined between 7° S and 18° N, while regions above and below these latitudes are relatively dry. This pattern of rainfall is mainly associated with the occurrence of mesoscale convective systems (d'Amato and Lebel, 1998; Jenkins et al., 2005). Two rainfall maxima are located around the Cameroon Mountains and Ethiopian Highlands which are associated with local orographic features. The model captures the general patterns of the observed rainfall distribution, in particular the ITCZ position and intensity. However, rainfall over southern Sudan, central Africa and the Ethiopian Highlands is overestimated. Also, the monsoon rain belt appears narrower in the model than in the observational data sets, as indicated by the negative precipitation biases north and south of the main rain belt. In general, the performance of our Reg-TB configuration appears to be in line with previous studies performed using the RegCM system in various configurations and domains (Sun et al., 1999; Pal et al., 2007; Anyah and Semazzi, 2007; Sylla et al., 2010b; Steiner et al., 2009; Zaroug et al., 2013) or with other regional modelling systems (e.g., Vizy and Cook, 2002; Nikulin et al., 2012; Paeth et al., 2005; Gallée et al., 2004; Flaounas et al., 2010; Druyan et al., 2008).

3.2 Temperature

The seasonal average of JJAS 2 m temperature for 1982 to 2009 is compared to CRU observations in Fig. 3. The lowest temperatures are found mostly over the mountainous areas of Cameroon and Ethiopian Highlands, Tanzania and South Kenya, while the warmest areas are confined between 15° N and 27° N, with larger values over the Sahara. Reg-TB (Fig. 3a) reproduces this spatial pattern but it shows a systematic cold bias of a few degrees in the convective regions of East Africa (Fig. 3b), Nigeria, Algeria and Libya. This cold bias over tropical and equatorial Africa has been a persistent feature in RegCM, as also found for example in the experiments of Sylla et al. (2010b) and Coppola et al. (2012), although the magnitude of the bias is somewhat reduced in our simulation. It should be stressed that the CRU observations are possibly affected by large uncertainties in this region due to the lack of observing stations, particularly in remote and mountainous areas (Mitchell et al., 2004). In addition, surface temperature depends on many parameters, including the presence of dust and aerosols. Given these uncertainties, we assess that a model bias of a few degrees is acceptable for this study.

3.3 Outgoing Long-Wave Radiation (OLR)

Figure 4 compares simulated and observed (NOAA) averaged JJAS OLR, which is essentially a measure of cloudiness. Both the model result shown in Fig. 4a and the observation result (not shown here) exhibit larger OLR values in North Africa because of small amounts of cloud cover, with correspondingly low OLR over the ITCZ. The model tends to overestimate the OLR over the Congo Basin (Fig. 4b) as a result of an underestimation of cloudiness over this region, a result which is in line with previous applications of the model (Zaroug et al., 2013; Sylla et al., 2010a, b). Slight overestimates are found over the Sahara and the Greater Horn of Africa (Fig. 4b), but in general the model captures well the general observed features of the OLR pattern in both magnitude and spatial extent.

3.4 Low-level circulation, Tropical Easterly Jet and African Easterly Jet

The spatial patterns of average JJAS low level (925 mb) circulation are shown in Fig. 5a for the ERA Interim reanalysis
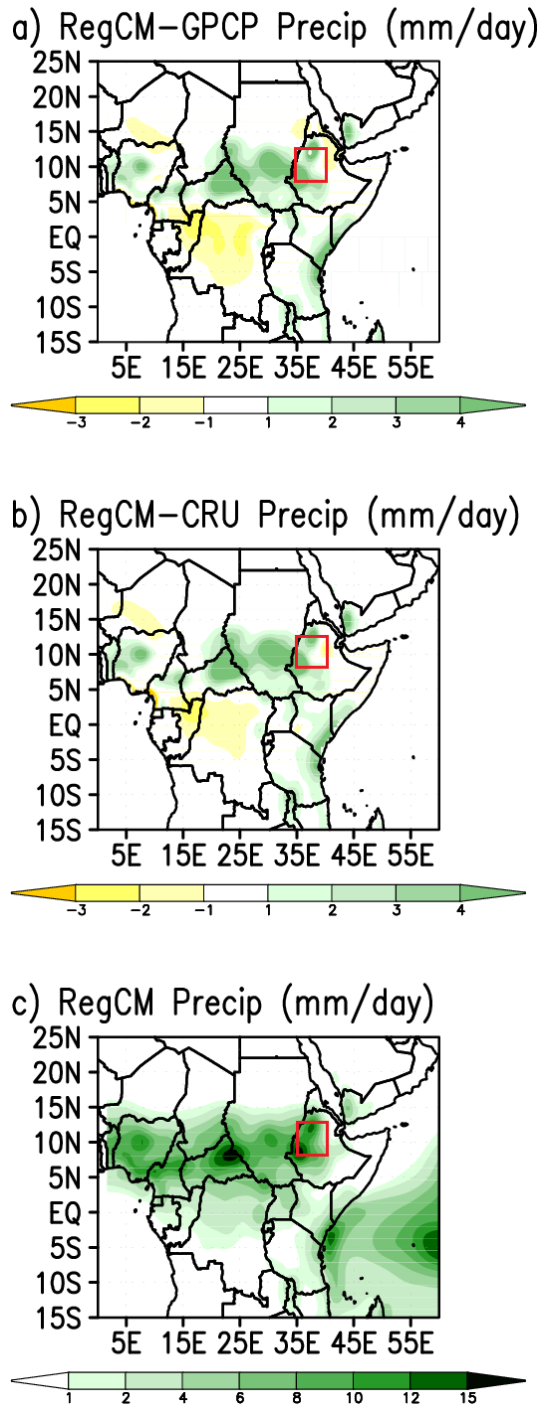
Figure 2. Averaged precipitation (in mm day^{-1}) for JJAS 1982–2009: **(a)** Reg-TB minus CRU, **(b)** Reg-TB minus GPCP, and **(c)** RegCM. Model data are ensemble averages.
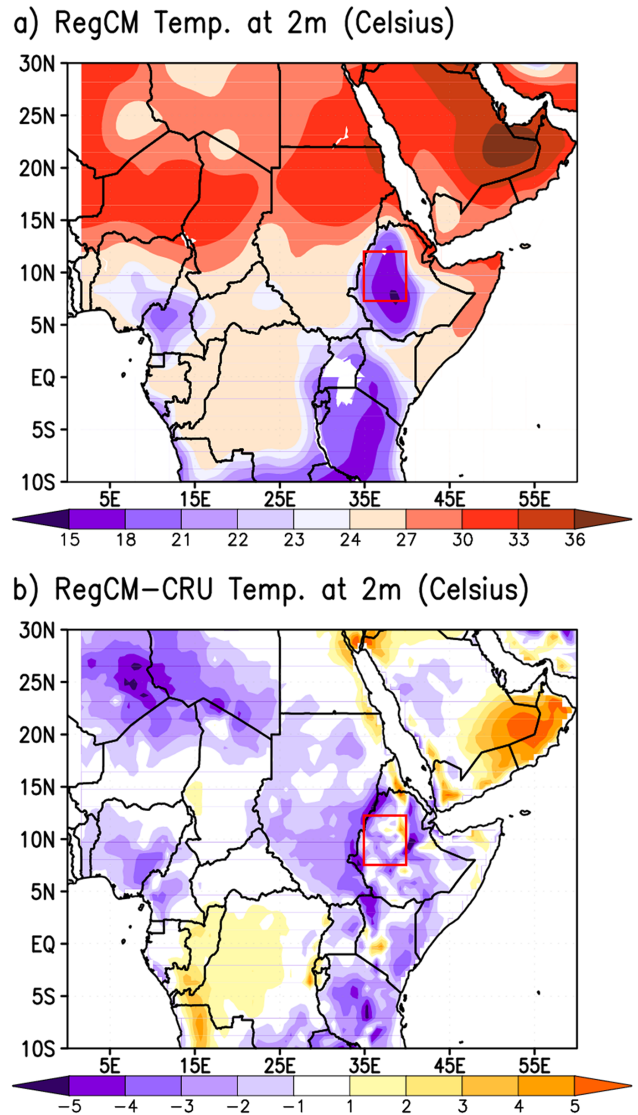

Figure 3. Averaged 2 m air temperature (in °C) for JJAS 1982–2009: **(a)** Reg-TB, **(b)** Reg-TB minus CRU. Model data are ensemble averages.

and Fig. 5b for the Reg-TB simulation. Direct observations of the low-level wind over the region are not available, and thus we use here the reanalysis product for evaluating the model. Overall, the model reproduces well the main features of the mean low-level circulation, such as the low-level mon-

soon flow over North Africa, the northerly Harmattan flow over East Africa, and the southeasterly flow over the Horn of Africa.

The Tropical Easterly Jet (TEJ), which affects the north African climate variability (Chen and Van Loon, 1987), develops between 200 and 150 mb in the upper troposphere over India in response to a large meridional thermal gradient and settles during the northern summer Asia monsoon season between the Tibetan Highlands and the Indian Ocean (Fontaine and Janicot, 1992; Koteswaram, 1958; Chen and van Loon, 1987). It stretches from the Indochina peninsula, across the African continent, to the tropical Atlantic (Wu et al., 2009), and it is linked to anomalous SSTs on a planetary scale (Chen and van Loon, 1987).
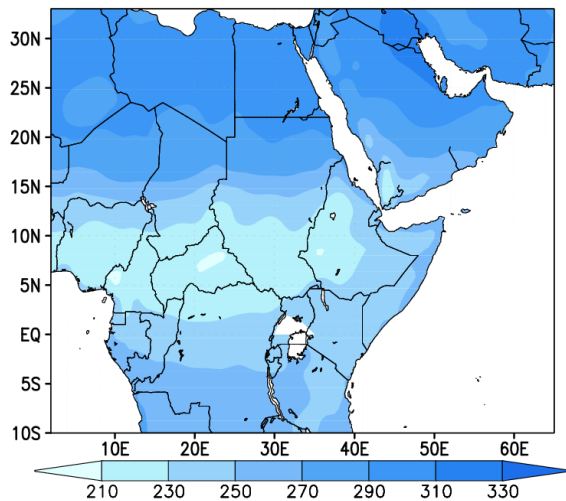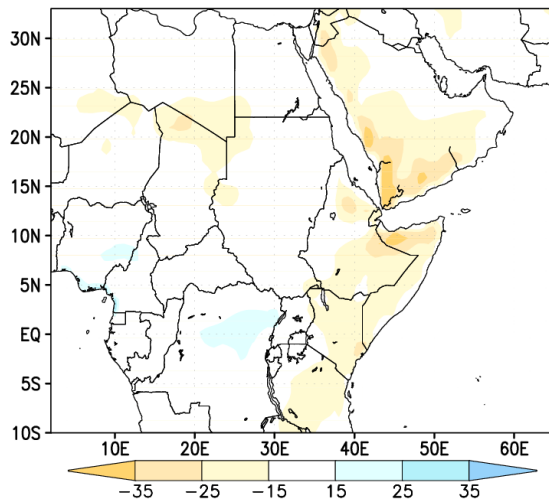
a) RegCM OLR (W/m2)

b) RegCM OLR-NOAA OLR (W/m2)

Figure 4. Averaged outgoing long-wave radiation (in W m^{-2}) for JJAS 1982–2009: **(a)** Reg-TB OLR, **(b)** Reg-TB OLR minus NOAA OLR. Model data are ensemble averages.

Figure 6 shows that the TEJ in the ERA Interim reanalysis is confined between 3 and 17° N with a core speed exceeding 15 m s^{-1}. The band of the jet decreases gradually from East Africa to West Africa. In fact, the highest wind speed of about 18 m s^{-1} occurs over the Horn of Africa and the western Indian Ocean, while the lowest speeds of about 6 m s^{-1} are found over Niger. Reg-TB reproduces well the structure of the TEJ shown in the ERA Interim reanalysis, capturing both the location and intensity of the jet, although the core of the jet extends somewhat westward and further into Sudan compared to ERA-Interim.

Another main feature of the African monsoon climate is the African Easterly Jet, which results mainly from the vertical inversion (around 600–700 mb) of the meridional tem-

perature gradient between the Sahara and equatorial Africa due to the existence of strong surface baroclinicity (Cook, 1999; Steiner et al., 2009) associated with deep atmospheric convection (Thorncroft and Blackburn, 1999; Sylla et al., 2010b). Figure 6c shows the ERA-Interim JJAS zonal wind at 600 mb. It is confined approximately between 7° N and 20° N extending from Chad to the Atlantic Ocean with a core speed ranging from 11 to 13 m s^{-1} located over West Africa. Again, Reg-TB simulates reasonably well both the strength and location of the African Easterly Jet (AEJ) (Fig. 6d).

In summary, the analysis presented in this section indicates that Reg-TB produces a realistic simulation of the climatology of the main dynamical and thermodynamical features of East African climate. In the next section we can thus turn our attention to the connections between ENSO and the hydroclimate of the upper Nile River Basin.

4 ENSO connections with East African climate

4.1 Difference between La Niña and El Niño years

Figure 7 provides an assessment of the capability of the observational GPCP data set to capture the differences in East African climate between La Niña and El Niño years. The GPCP data were analysed for the same 28 years used in the simulations, 1982–2009, and 5 La Niña and El Niño years included in this period were selected. The average precipitation for the 5 La Niña years (1988, 1998, 1999, 2007 and 2008), the 5 El Niño years (1982, 1983, 1987, 1992 and 2002) along with their difference are shown in the upper, middle and lower panels of Fig. 7, respectively. The GPCP data show a strong signal of increased (decreased) rainfall during La Niña (El Niño) years over the Sahel region up to about 18° N, including the upper catchment of the Nile River. This result agrees qualitatively with previous observational analyses, which suggested that La Niña years are associated with above normal rainfall and El Niño years with below normal rainfall in the upper catchment of the Blue Nile (Eltahir, 1996; Wang and Eltahir, 1999; Amarasekera et al., 1997; De Putter et al., 1998; Camberlin et al., 2001; Abtew et al., 2009).

Figure 8 shows the corresponding fields averaged over the nine-member ensemble of Reg-TB simulations. The nine members were first averaged for each month of the 28 simulated years (1982–2009), and then the 5 La Niña and El Niño years were selected as in the observational analysis. The rainfall was then averaged for the rainy season (JJAS) and for the 5 La Niña and El Niño years to obtain ensemble-averaged values. It can be seen that the model captures the positive La Niña minus El Niño precipitation signal over the Sahel region, although this is less intense than in the observations and does not extend as far north. In addition, the model shows a negative signal in the region just North of Lake Victoria. The results of each ensemble member were also analysed
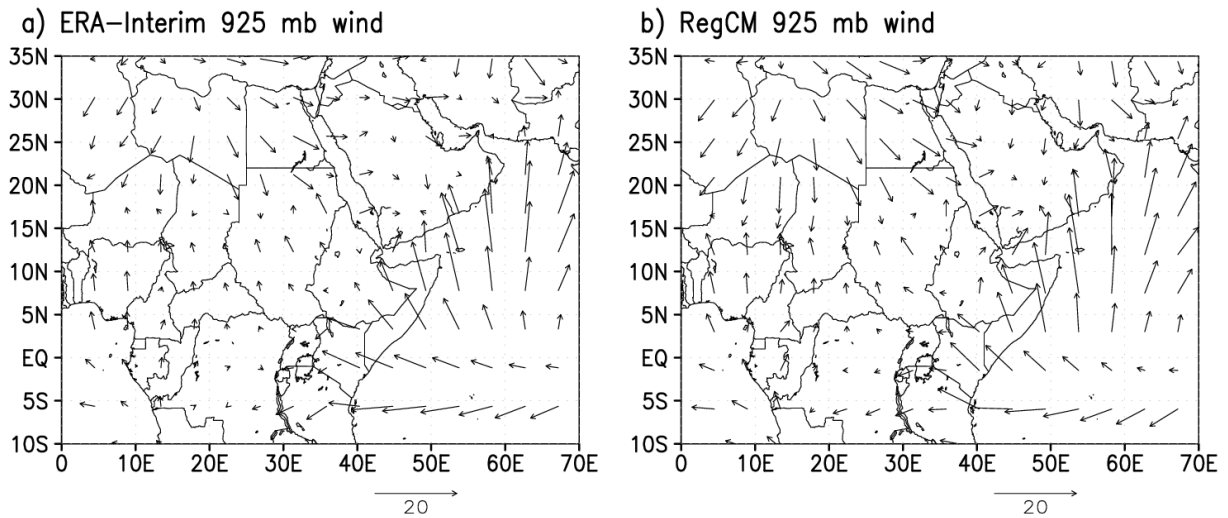
Figure 5. Averaged 925 mb wind vector for JJAS 1982–2009: **(a)** ERA-Interim, **(b)** Reg-TB (ensemble average).
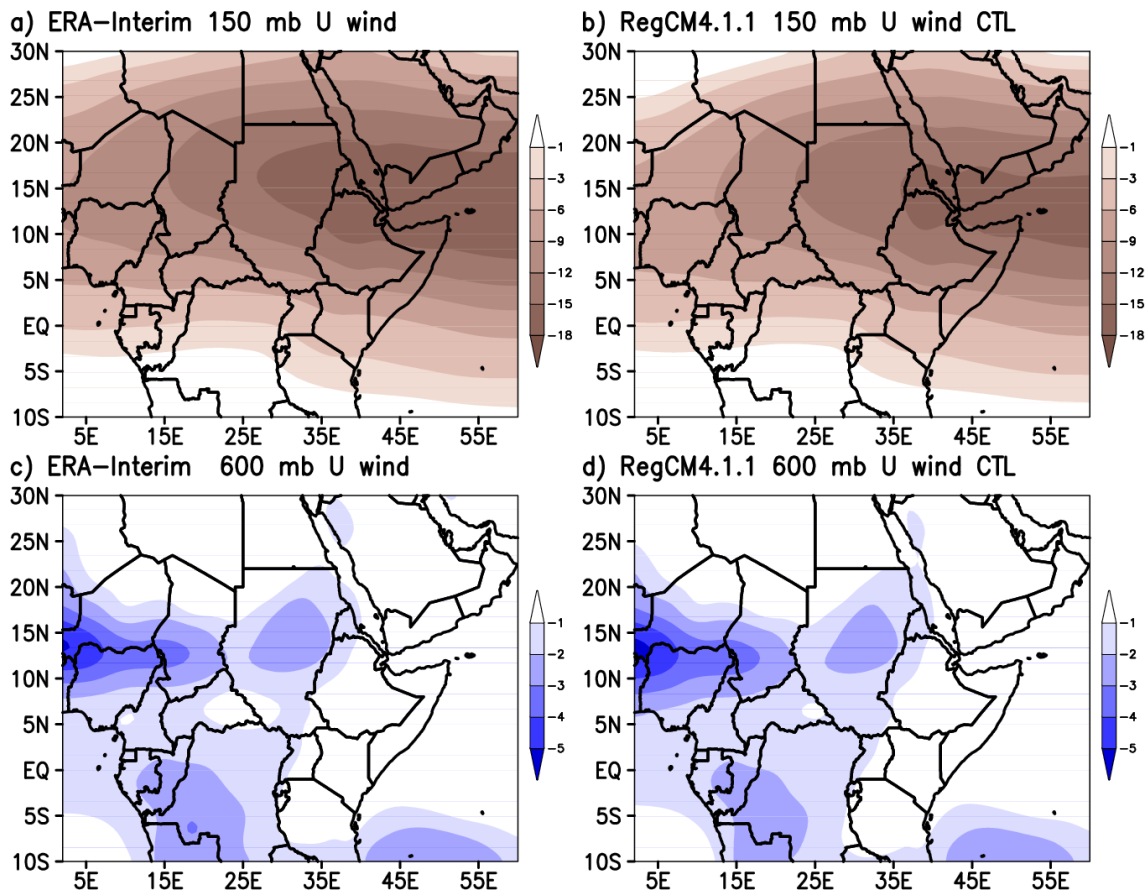

Figure 6. Averaged zonal wind (in m s^{-1}) for JJAS 1982–2009: **(a)** ERA Interim at 150 mb, **(b)** Reg-TB at 150 mb, **(c)** ERA Interim at 600 mb, and **(d)** Reg-TB at 600 mb. Model data are ensemble averages.
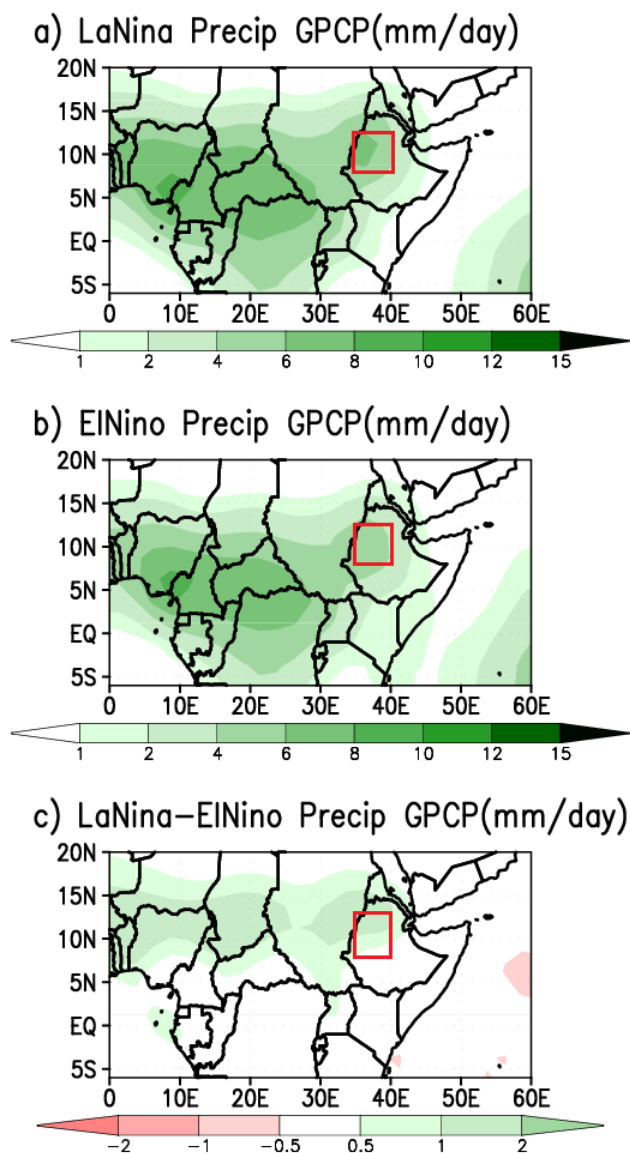
Figure 7. GPCP rainfall during JJAS for **(a)** 5 La Niña years (1988, 1998, 1999, 2007 and 2008), **(b)** 5 El Niño years (1982, 1983, 1987, 1992 and 2002), and **(c)** the difference between La Niña years and El Niño years.

Figure 8. Ensemble average Reg-TB JJAS rainfall for **(a)** 5 La Niña years (1988, 1998, 1999, 2007 and 2008), **(b)** 5 El Niño years (1982, 1983, 1987, 1992 and 2002), and **(c)** the difference between La Niña years and El Niño years.

(not shown) and they showed a substantial variability across different members, which results in the average signal over the Sahel being weakened. Notwithstanding this problem, the model captured the ENSO-forced main positive signal over the Sahel band and the upper Nile catchment.

We also calculated the same El Niño and La Niña precipitation signals (i.e. using the same 5 El Niño and La Niña years as in Figs. 7 and 8) from the ERA-Interim reanalysis (Fig. 9). Surprisingly, we find a pronounced negative La Niña minus El Niño precipitation signal over the Sahel, in disagreement with the GPCP observations, along with shifted rainfall maxima in the upper Blue Nile area. We thus
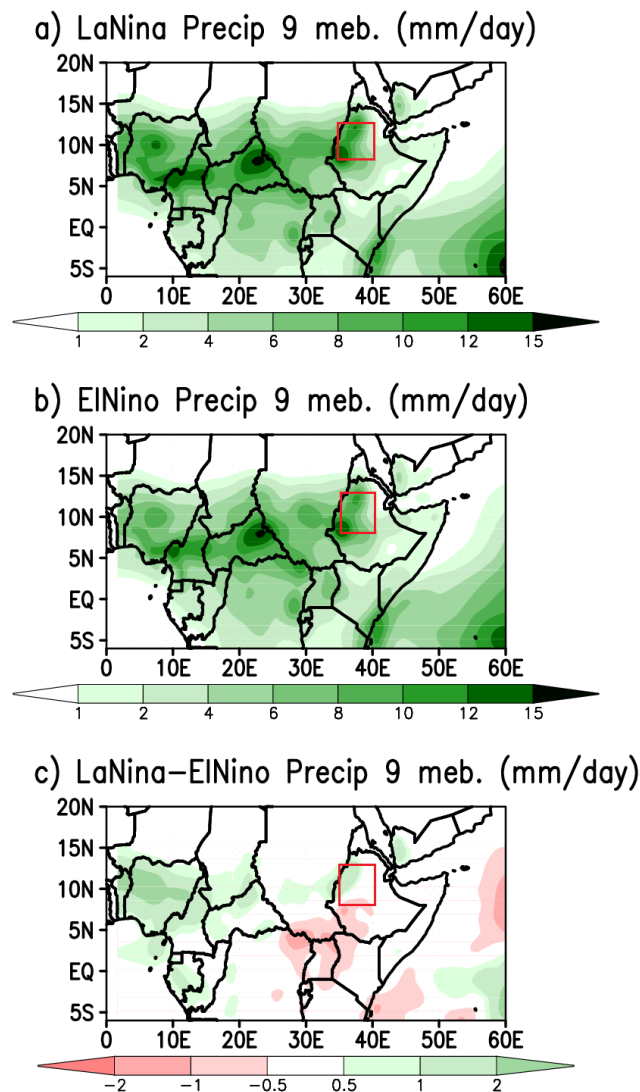
conclude that the internal physics of the Reg-TB corrected the representation of the teleconnection between ENSO and African precipitation found in ERA-Interim.

4.2 Correlation between rainfall anomalies over the Ethiopian highlands and SST anomalies in the Niño 3.4 region

Figure 10 shows the correlation between the ensemble average rainfall anomalies over the upper Nile river catchment during JJAS and the SST anomalies in the Niño 3.4 region during 3-month periods from January–February–March (JFM) to October–November–December (OND) calculated
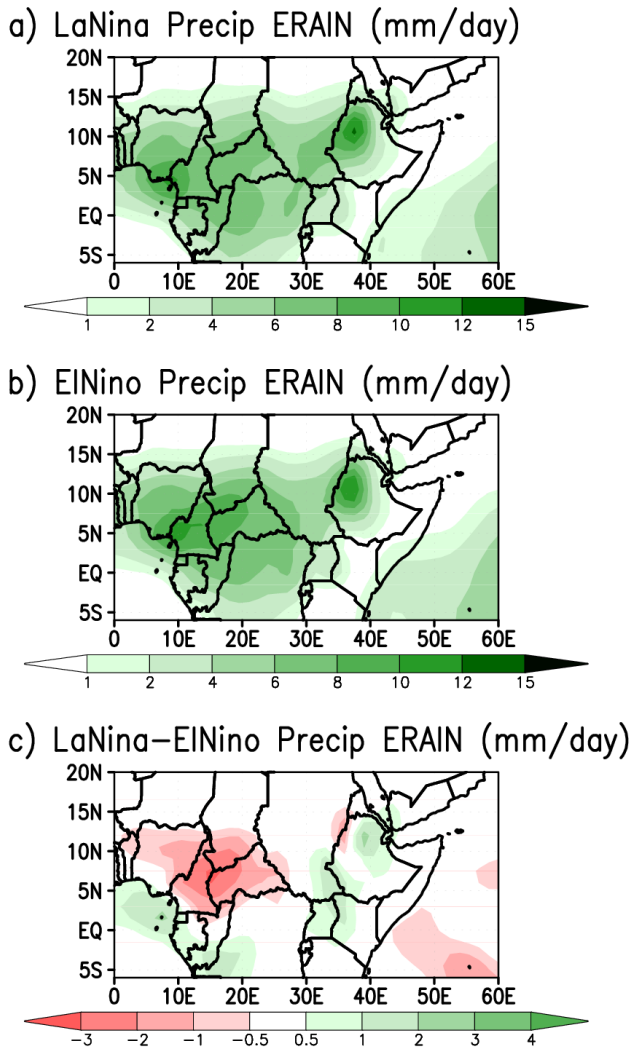
Figure 9. ERA Interim JJAS rainfall for (a) 5 La Niña years (1988, 1998, 1999, 2007 and 2008), (b) 5 El Niño years (1982, 1983, 1987, 1992 and 2002), and (c) the difference between La Niña years and El Niño years.

over a period of 28 years (1982 to 2009) using the equation

$$\mathrm{Correl}\,(X,Y) = \frac{\sum (x - \bar{x})\,(y - \bar{y})}{\sqrt{\sum (x - \bar{x})^2 \sum (y - \bar{y})^2}}, \qquad (1)$$

where $\bar{x}$ is the mean of the variable x (i.e. Niño 3.4 anomalies) and $\bar{y}$ is the mean of variable y (i.e. rainfall anomalies over the Ethiopia Highlands). The correlations are negative for all SST seasons, with the highest value of -0.62 during AMJ and the lowest of -0.35 in OND. Figure 10 also shows the same SST–precipitation correlations calculated for the GPCP and CRU observation data sets for the same 28 years. We first note the substantial difference across the two data sets, with GPCP shifting the correlation maximum to the MJJ period, which confirms the uncertainties found in precipitation observations over this region (e.g. Sylla et al., 2013).
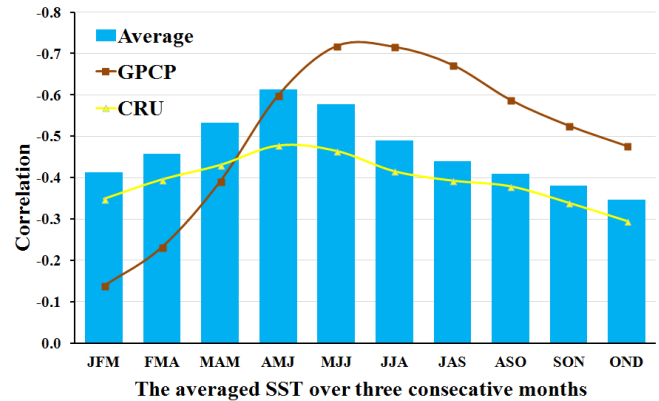

Figure 10. Correlation between rainfall anomalies over the Ethiopian Highlands (Reg-TB ensemble average, GPCP and CRU) and SST anomalies over the Pacific Ocean in the Niño 3.4 region.
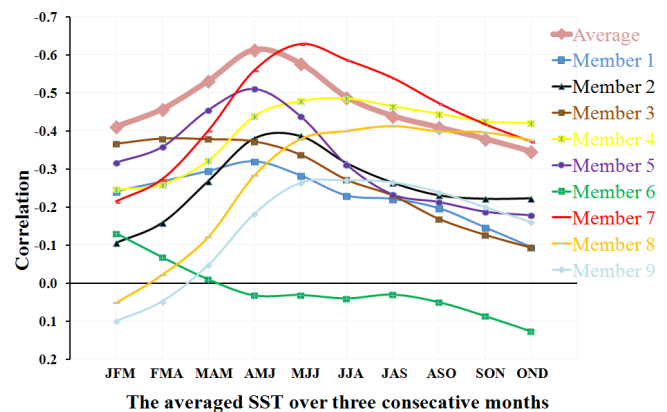

Figure 11. Correlation between rainfall anomalies over the Ethiopian Highlands (Reg-TB ensemble average and each individual ensemble member) and SST anomalies over the Pacific Ocean in the Niño 3.4 region.

The model correlations are in good agreement with the CRU ones, both in terms of magnitude and timing, thereby indicating a good performance by the model despite the observational uncertainties.

Figure 11 shows the corresponding SST–precipitation correlations (for the period 1982–2009) for each ensemble member. We find a considerable spread across members in both magnitude and timing of the correlation maximum. Most members, however, show values generally in line with the observational uncertainty with the prominent exception of member 6, which is very far from observations. An important conclusion from this analysis is that the internal variability of the tropical band model is high and that ensembles of simulations are needed to capture the atmospheric response to ENSO (Shukla et al., 2000). Table 1 shows the significance of the correlations at the 95 % confidence level, which was calculated for each ensemble member and for the average of the nine members. Members 1, 6 and 9 were below the 95 %
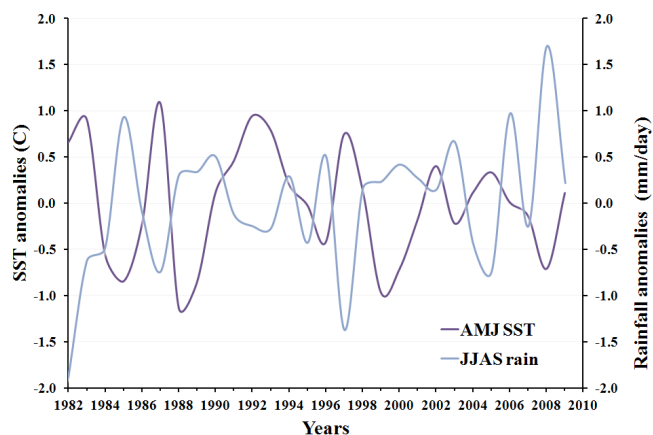
Figure 12. SST anomalies during AMJ in the Niño 3.4 region and ensemble average Reg-TB rainfall anomalies in the upper catchment of the Blue Nile.

confidence level for all the seasons. The correlation is not significant for nearly all the members in JFM and FMA, a result in line with a recent study by Zaroug et al. (2014). The average of the nine members shows a highly significant correlation when compared with each ensemble member. The confidence test for the GPCP and CRU were calculated in Zaroug et al. (2014), who confirmed the strong impact of ENSO anomalies on the rainfall of the Ethiopia Highlands.

Finally, Figure 12 shows the time evolution of AMJ SST anomalies and ensemble average JJAS precipitation over the upper Blue Nile river catchment, further evidencing the negative correlation between these two variables. The coefficient of determination (R^2) for the linear fit between Niño 3.4 anomalies in different seasons and the JJAS averaged simulated rainfall anomalies at the upper catchment of the Blue Nile for the period 1982–2009 is shown in Table 2. AMJ shows the highest coefficient of determination. The same calculation was completed for each ensemble member (not shown here) and member 7 showed the largest R^2 values. In a recent study, Zaroug et al. (2014) showed that the Blue Nile discharge showed the highest correlation for drought events with the Niño 3.4 SST during AMJ, a result which appears to be in line with Fig. 10. These results support the use of Niño 3.4 SST during AMJ for seasonal forecasting of hydroclimate conditions in the upper catchment of the Blue Nile.

4.3 Regression analysis of Niño 3.4 index onto summer rainfall over the Sahel and East Africa

In this section we investigate further the relationship between ENSO and summer rainfall over the Sahel through a regression analysis between SST in the Niño 3.4 region and rainfall in the summer for both the model and the GPCP observations. Figure 13 presents the regression of the JJA Niño 3.4 index onto the JJA GPCP rainfall from 1982 to 2009. The term b of the linear regression ($y = a + bx + e$) is calculated

using the equation

$$b = \frac{\sum (x_i - \bar{x})(y_i - \bar{y})}{\sum (x_i - \bar{x})^2},\tag{2}$$

where $\bar{x}$ is the mean of the variable x (i.e. Niño 3.4 anomalies) values and $\bar{y}$ is the mean of the variable y (i.e. rainfall anomalies). Niño 3.4 has an impact on many regions around the world, with a high positive signal in the equatorial Pacific and a negative signal over India, Southeast Asia and the northern part of South America. Figure 14 zooms over the Sahel and East Africa region and in the observations shows a negative signal over most of the Sahel and equatorial Africa regions, with a maximum over the Ethiopia Highlands.

The same regression analysis for the model ensemble average precipitation shows that, by and large, it reproduces the main features of the observed signal. Specifically, it reproduces the negative signal over the Sahel and East Africa region. Over equatorial Africa and the Congo Basin, the model shows areas of small positive signal not found in the observations. However, as already mentioned, observed precipitation over those areas may be characterized by large uncertainties due to lack of observing stations.

5 Conclusions

In this study we used the tropical band version of the RegCM4 system (Giorgi et al., 2012; Coppola et al., 2012) to simulate the observed statistical relationship between ENSO and the summer rainfall regime of the Sahel and East Africa, with a focus on the upper Blue Nile basin. Towards this objective an ensemble of nine 28 yr long simulations was completed for a domain covering the entire tropical belt between ∼ 45° S and ∼ 45° N, driven by observed SST and north–south boundary conditions from the ERA-Interim reanalysis.

The climatology of Reg-TB over the Sahel and East Africa region was first evaluated against observations and the reanalysis product. It was shown that the model performs reasonably well in reproducing the observed climatology of temperature, rainfall, outgoing long-wave radiation and large-scale atmospheric circulation features. For example, the model captured well the rain belt, as well as the peaks over the Ethiopian, Guinea and Cameroon Highlands. In fact, this simulation even outperformed in some aspects previous applications of this model over the region (Sylla et al., 2010b, Zaroug et al., 2013). In addition, the lower-level and large-scale circulation features affecting the monsoon (TEJ, AEJ) were realistically captured.

We then analysed the ability of the model to reproduce the observed teleconnections between the Pacific SST and summer precipitation over the Sahel, East Africa and upper Nile River catchment. The model (average of nine members) was able to reproduce the observed negative correlation between the Niño 3.4 SST and precipitation over the focus regions, even outperforming the ERA-Interim reanalysis. It
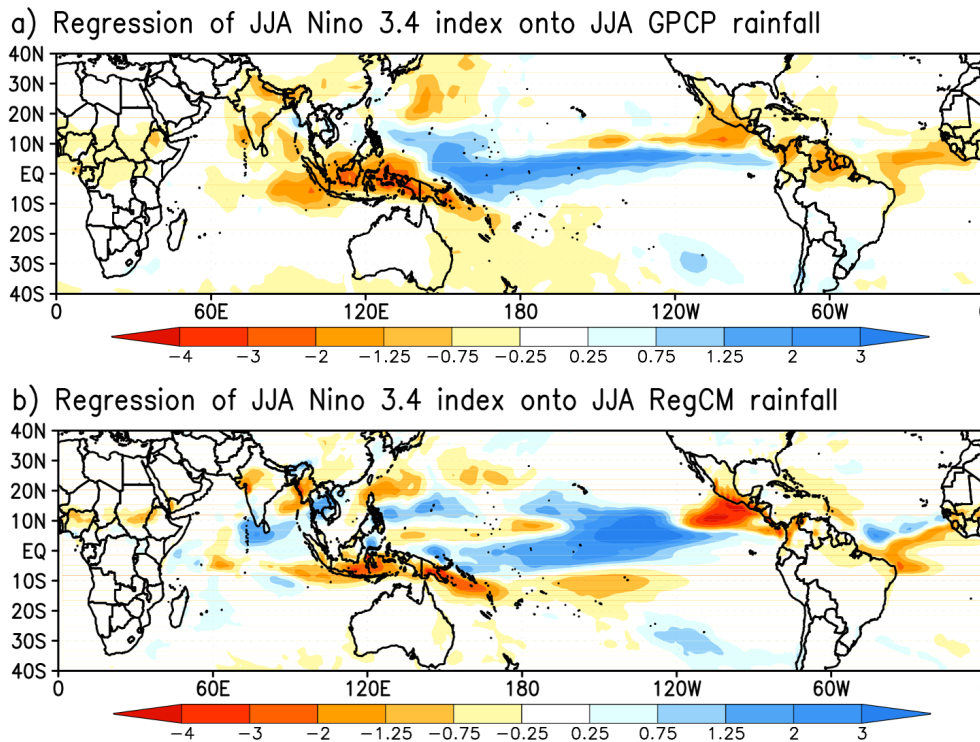
a) Regression of JJA Nino 3.4 index onto JJA GPCP rainfall

b) Regression of JJA Nino 3.4 index onto JJA RegCM rainfall

Figure 13. Regression of JJA Niño 3.4 index onto JJA rainfall for 1982–2009. **(a)** GPCP; **(b)** Reg-TB ensemble average.

Table 1. 95 % significance test of the correlation between Niño 3.4 anomalies and rainfall at the upper catchment of the Blue Nile (see Fig. 1) for the nine simulation members and for the ensemble average. The correlation is calculated over the period 1982–2009.

Rainfall	Season of Niño 3.4									
	JFM	FMA	MAM	AMJ	MJJ	JJA	JAS	ASO	SON	OND
M1	−1.268	−1.411	−1.57	−1.721	−1.502	−1.204	−1.154	−1.021	−0.752	−0.482
M2	−0.54	−0.816	−1.42	−2.101	−2.139	−1.694	−1.394	−1.208	−1.158	−1.165
M3	−2.004	−2.092	−2.08	−2.043	−1.825	−1.436	−1.201	−0.87	−0.65	−0.473
M4	−1.296	−1.374	−1.74	−2.497	−2.786	−2.834	−2.681	−2.537	−2.399	−2.367
M5	−1.703	−1.954	−2.603	−3.022	−2.487	−1.671	−1.221	−1.115	−0.976	−0.927
M6	−0.673	−0.348	−0.049	0.165	0.159	0.205	0.154	0.257	0.444	0.653
M7	−1.119	−1.446	−2.229	−3.441	−4.118	−3.692	−3.262	−2.733	−2.34	−2.04
M8	0.263	−0.114	−0.624	−1.506	−2.088	−2.226	−2.312	−2.219	−2.201	−2.071
M9	0.508	0.241	−0.246	−0.951	−1.399	−1.435	−1.406	−1.259	−1.042	−0.833
Av.	−2.306	−2.627	−3.204	−3.962	−3.607	−2.858	−2.498	−2.292	−2.095	−1.887

Italic: below the critical value of −2.056 (not significant).
Non italic: above the critical value of −2.056 (significant).

also showed the highest correlation of SST and summer precipitation over the Ethiopia Highlands during AMJ (−0.62), in line with previous observational studies (Zaroug et al., 2014). This result suggests that AMJ SSTs over the Niño 3.4 region can be a useful predictor in seasonal (JJAS) precipitation forecasting over East Africa and the Blue Nile region.

We finally investigated the SST–precipitation correlations in the individual ensemble members and found a wide spread across the ensemble members, which however reproduced the basic negative correlation pattern (except for one ensemble member). This confirms the need to perform ensembles of simulations to capture robust ENSO teleconnection signals (Shukla et al., 2000). Overall, our analysis provides encouraging indications towards the use of the Reg-TB configuration in seasonal forecasting, climate change and teleconnection studies over East Africa region.

Table 2. Coefficient of determination (R^2) for the linear fit between Niño 3.4 in different seasons and the JJAS averaged simulated rainfall anomalies at the upper catchment of the Blue Nile for the period 1982–2009.

Rainfall anomalies	Season of Niño 3.4 anomalies									
	JFM	FMA	MAM	AMJ	MJJ	JJA	JAS	ASO	SON	OND
Average	0.17	0.21	0.28	0.38	0.33	0.24	0.19	0.17	0.14	0.12
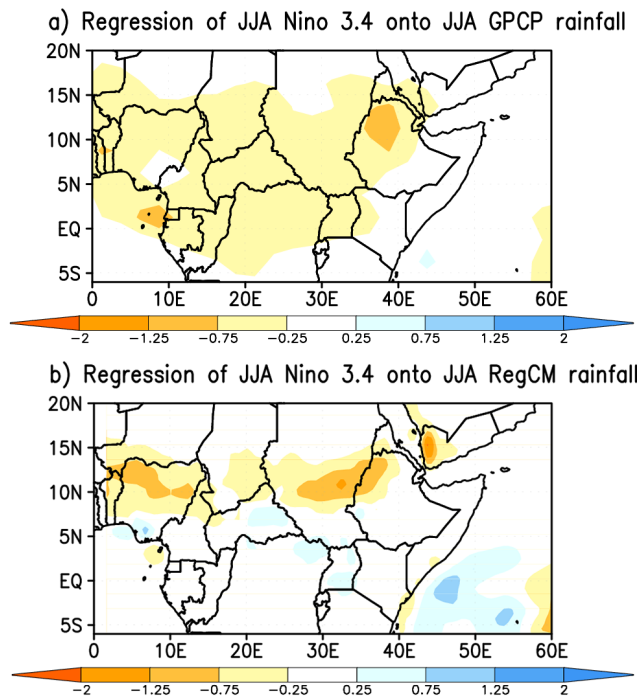
Figure 14. As Fig. 13 but for the Sahel and equatorial Africa region: **(a)** GPCP; **(b)** Reg-TB ensemble average.

References

Abtew, W., Melesse, A. M., and Dessalegne, T.: El Niño Southern Oscillation link to the Blue Nile River Basin hydrology, Hydrol. Process., 23, 3653–3660, 2009.

Amarasekera, K. N., Lee, R. F., Williams, E. R., and Eltahir, E. A. B.: ENSO and the natural variability in the flow of tropical rivers, J. Hydrol., 200, 24–39, 1997.

Anyah, R. O. and Semazzi, F. H. M.: Variability of East African rainfall based on multiyear RegCM3 simulations, Int. J. Climatol., 27, 357–371, 2007.

Camberlin, P., Janicot, S., and Poccard, I.: Seasonality and atmospheric dynamics of the teleconnection between African rainfall and tropical sea surface temperature: Atlantic vs. ENSO, Int. J. Climatol., 21, 973–1005, 2001.

Chen, T. C. and van Loon, H.: Interannual variation of the tropical easterly jet, Mon. Weather Rev., 115, 1739–1759, 1987.

Cook, K. H.: Generation of the African easterly jet and its role in determining West African precipitation, J. Climate, 12, 1165–1184, 1999.

Coppola, E., Giorgi, F., Mariotti, L., and Bi, X.: RegT-Band: A tropical band version of RegCM4, Clim. Res., 52, 115–133, 2012.

D'amato, N. and Lebel, T.: On the characteristics of the rainfall events in the Sahel with a view to the analysis of climatic variability, Int. J. Climatol., 18, 955–974, 1998.

Dee, D. P., Uppala, S. M., Simmons, A. J., Berrisford, P., Poli, P., Kobayashi, S., Andrae, U., Balmaseda, M. A., Balsamo, G., Bauer, P., Bechtold, P., Beljaars, A. C. M., van de Berg, L., Bidlot, J., Bormann, N., Delsol, C., Dragani, R., Fuentes, M., Geer, A. J., Haimberger, L., Healy, S. B., Hersbach, H., Hólm, E. V., Isaksen, L., Kållberg, P., Köhler, M., Matricardi, M., McNally, A. P., Monge-Sanz, B. M., Morcrette, J. J., Park, B. K., Peubey, C., de Rosnay, P., Tavolato, C., Thépaut, J. N., and Vitart, F.: The ERA-Interim reanalysis: configuration and performance of the data assimilation system, Q. J. Roy. Meteor. Soc., 137, 553–597, doi:10.1002/qj.828, 2011.

De Putter, T., Loutre, M., and Wansard, G.: Decadal periodicities of Nile River historical discharge (AD 622–1470) and climatic implications, Geophys. Res. Lett., 25, 3193–3196, 1998.

Diaz, H. F., Hoerling, M. P., and Eischeid, J. K.: ENSO variability, teleconnections and climate change, Int. J. Climatol., 21, 1845–1862, 2001.

Dickinson, R. E., Henderson-Sellers, A., Kennedy, P. J., and Wilson, M. F.: Biosphere–atmosphere transfer scheme (BATS) version 1e as coupled to the NCAR Community Climate Model, NCAR Tech. Note, NCAR/TN387+ STR., 1993.

Druyan, L. M., Fulakeza, M., and Lonergan, P.: The impact of vertical resolution on regional model simulation of the west African summer monsoon, Int. J. Climatol., 28, 1293–1314, 2008.

Dumont, H. J.: The Nile: origin, environments, limnology and human use, Monog. Biol., Vol. 89, Springer Netherlands, 2009.

Elagib, N. A. and Elhag, M. M.: Major climate indicators of ongoing drought in Sudan, J. Hydrol., 409, 612–625, 2011.

Eltahir, E. A. B.: El Niño and the natural variability in the flow of the Nile River. Water Res., 32, 131–137, 1996.

Emanuel, K.: A scheme for representing cumulus convection in large-scale models, J. Atmos. Sci., 48, 2313–2335, 1991.

Flaounas, E., Bastin, S., and Janicot, S.: Regional climate modelling of the 2006 West African monsoon: sensitivity to convection and planetary boundary layer parameterisation using WRF, Clim. Dynam., 36, 1083–1105, 2011.

Fontaine, B. and Janicot, S.: Wind-field coherence and its variations over West Africa, J. Climate, 5, 512–524, 1992.

Gallée, H., Moufouma-Okia, W., Bechtold, P., Brasseur, O., Dupays, I., Marbaix, P., Messager, C., Ramel, R., and Lebel, T.: A high resolution simulation of a West African rainy season using a regional climate model, J. Geophys. Res., 109, D05108, doi:10.1029/2003JD004020, 2004.

Giorgi, F., Coppola, E., Solmon, F., Mariotti, L., Sylla, M. B., Bi, X., Elguindi, N., Diro, G. T., Nair, V., and Giuliani, G.: RegCM4: model description and preliminary tests over multiple CORDEX domains, Clim. Res., 52, 7–29, doi:10.3354/cr01018, 2012.

Gissila, T., Black, E., Grimes, D. I. F., and Slingo, J. M.: Seasonal forecasting of the Ethiopian summer rains, Int. J. Climatol., 24, 1345–1358, 2004.

Grell, G. A.: Prognostic evaluation of assumptions used by cumulus parameterizations, Mon. Weather Rev., 121, 764–787, 1993.

Holton, J. R., Dmowska, R., and Philander, S. G.: El Niño, La Niña, and the southern oscillation, Academic press, 1989.

Holtslag, A. A. M., De Bruijn, E. I. F., and Pan, H. L.: A high resolution air mass transformation model for short-range weather forecasting, Mon. Weather Rev., 118, 1561–1575, 1990.

Huffman, G. J., Bolvin, D. T., and Adler, R. F.: GPCP Version 2.2 Combined Precipitation Data set, WDC-A, NCDC, Asheville, NC, 2011.

Jenkins, G. S., Gaye, A. T., and Sylla, B.: Late 20th century attribution of drying trends in the Sahel from the Regional Climate Model (RegCM3), Geophys. Res. Lett., 32, L22705, doi:10.1029/2005GL024225, 2005.

Kiehl, J. T., Hack, J. J., Bonan, G. B., Boville, B. A., Briegleb, B. P., Williamson, D. L., and Rasch, P. J.: Description of the NCAR Community Climate Model (CCM3), NCAR Technical Note NCAR/TN-420+STR, doi:10.5065/D6FF3Q99, 1996.

Koteswaram, P.: The Easterly Jet Stream in the tropics, Tellus, 10, 43–57 1958.

Mitchell, T. D., Carter, T. R., Jones, P. D., Hulme, M., and New, M.: A comprehensive set of high resolution grids of monthly climate for Europe and the globe: the observed record (1901–2000) and 16 scenarios (2001–2100), Tyndall Centre for Climate Change Research Working Paper, 55, 25 pp., 2004.

Müller, W. A. and Roeckner, E.: ENSO teleconnections in projections of future climate in ECHAM5/MPI-OM, Clim. Dynam., 31, 533–549, 2008.

Nikulin, G., Jones, C., Samuelsson, P., Giorgi, F., Sylla, M. B., Asrar, G., Baüchner, M., Christensen, O. B., Déqué, M., and Fernandez, J.: Precipitation climatology in an ensemble of CORDEX-Africa regional climate simulations, J. Climate, 25, 6057–6078, doi:10.1175/JCLI-D-11-00375.1,2012.

Osman, Y. Z. and Shamseldin, A. Y.: Qualitative rainfall prediction models for central and southern Sudan using El Niño–Southern Oscillation and Indian Ocean sea surface temperature indices, Int. J. Climatol., 22, 1861–1878, 2002.

Osman, Y. Z., Shamseldin, A. Y., and Abdo, G. M.: El Niño–Southern Oscillation and rainfall variability in central and southern Sudan, Water Int., 26, 177–184, 2001.

Paeth, H., Born, K., Podzun, R., and Jacob, D.: Regional dynamical downscaling over West Africa: model evaluation and comparison of wet and dry years, Meteorol. Z., 14, 349–368, 2005.

Pal, J. S., Eltahir, E. A. B., and Small, E. E.: Simulation of regional-scale water and energy budgets- Representation of subgrid cloud and precipitation processes within RegCM, J. Geophys. Res., 105, 567–594, 2000.

Pal, J. S., Giorgi, F., Bi, X., Elguindi, N., Solmon, F., Rauscher, S. A., Gao, X., Francisco, R., Zakey, A., and Winter, J.: Regional climate modeling for the developing world: the ICTP RegCM3 and RegCNET, B. of the Am. Meteorol. Soc., 88, 1395–1409, 2007.

Reynolds, R. W., Smith, T. M., Liu, C., Chelton, D. B., Casey, K. S., and Schlax, M. G.: Daily high-resolution-blended analyses for sea surface temperature, J. Climate, 20, 5473–5496, 2007.

Ropelewski, C. F. and Halpert, M. S.: Global and regional scale precipitation patterns associated with the El Niño/Southern Oscillation, Mon. Weather Rev., 115, 1606–1626, 1987.

Segele, Z. T. and Lamb, P. J.: Characterization and variability of Kiremt rainy season over Ethiopia, Meteorol. and Atmos. Phys., 89, 153–180, 2005.

Seleshi, Y. and Zanke, U.: Recent changes in rainfall and rainy days in Ethiopia. Int. J. Climatol., 24, 973–983, 2004.

Shukla, J., Marx, L., Paolino, D., Straus, D., Anderson, J., Ploshay, J., and Kalnay, E.: Dynamical seasonal prediction, B. Am. Meteorol. Soc., 81, 2593–2606, 2000.

Steiner, A. L., Pal, J. S., Rauscher, S. A., Bell, J. L., Diffenbaugh, N. S., Boone, A., Sloan, L. C., and Giorgi, F.: Land surface coupling in regional climate simulations of the West African monsoon, Clim. Dynam., 33, 869–892, 2009.

Sun, L., Semazzi, F. H. M., Giorgi, F., and Ogallo, L. A.: Application of the NCAR regional climate model to eastern Africa. Part 1: simulation of the short rains of 1988, J. Geophys. Res., 104, 6529–6548, 1999.

Sylla, M. B., Dell'Aquila, A., Ruti, P. M., and Giorgi, F.: Simulation of the intraseasonal and the interannual variability of rainfall over West Africa with RegCM3 during the monsoon period, Int. J. Climatol., 30, 1865–1883, 2010a.

Sylla, M. B., Coppola, E., Mariotti, L., Giorgi, F., Ruti, P. M., Dell'Aquila, A., and Bi, X.: Multi year simulation of the African climate using a regional climate model (RegCM3) with the high resolution ERA-interim reanalysis, Clim. Dynam., 35, 231–247, 2010b.

Sylla, M., Giorgi, F., Coppola, E. and Mariotti, L.: Uncertainties in daily rainfall over Africa: assessment of gridded observation products and evaluation of a regional climate model simulation, Int. J. Climatol., 33, 1805–1817, 2013.

Thorncroft, C. D. and Blackburn, M.: Maintenance of the African easterly jet, Q. J. Roy. Meteor. Soc., 125, 763–786, 1999.

Vizy, E. K. and Cook, K. H.: Development and application of a mesoscale climate model for the tropics: Influence of sea surface temperature anomalies on the West African monsoon, J. Geophys. Res., 107, doi:10.1029/2001JD000686, 2002.

Wang, G. and Eltahir, E. A. B.: Use of ENSO information in medium-and long-range forecasting of the Nile floods, J. Climate, 12, 1726–1737, 1999.

Wu, M. L. C., Reale, O., Schubert, S. D., Suarez, M. J., Koster, R. D., and Pegion, P. J.: African Easterly Jet: Structure and Maintenance, J. Climate, 22, 4459–4480, 2009.

Zaroug, M. A. H., Eltahir, E. A. B., and Giorgi, F.: Droughts and floods over the upper catchment of the Blue Nile and their connections to the timing of El Niño and La Niña events, Hydrol. Earth Syst. Sci., 18, 1239–1249, doi:10.5194/hess-18-1239-2014, 2014.

Zaroug, M. A., Sylla, M., Giorgi, F., Eltahir, E. A., and Aggarwal, P. K.: A sensitivity study on the role of the swamps of southern Sudan in the summer climate of North Africa using a regional climate model, Theoret. Appl. Climatol., 113, 63–81, 2013.